Original scientific paper
DOI: /10.5513/JCEA01/25.4.4385
Journal of Central European Agriculture, 2024, 25(4), p.1135-1147

Use of UAVs' multispectral images for sugar beet cultivars discrimination and yield estimation

Vasileios DRIMZAKAS–PAPADOPOULOS[1], Konstantinos NTOUROS[1,2] (✉), Constantine PAPATHEODOROU[1], Alexandros KONSTANTINIDIS[1]

[1] Department of Surveying Engineering & Geoinformatics, International Hellenic University, I.H.U. Serres Campus, Terma Magnesias str., 62124, Serres, Greece

[2] NubiGroup Geoservices & Research Private Company, Ymittou 27 str., 54453, Thessaloniki, Greece

✉ Corresponding author: konstantinos.d.ntouros@gmail.com

Received: April 30, 2024; Accepted: September 22, 2024

ABSTRACT

The significance of crop mapping using remote sensing data is increasingly recognized as a cornerstone for tackling global challenges such as food security and climate change, due to its role in providing accurate and timely information on crop distribution, essential for informed agricultural decision-making. The main objective of this study was to investigate the effectiveness of multispectral UAV imagery for discriminating between sugar beet cultivars and predicting yield. The specific objectives were: i Evaluation of the separability of spectral bands and vegetation indices for 25 sugar beet cultivars using histogram correlation analysis, and ii. Investigating potential correlations between vegetation indices and yield. The results showed the NIR spectral region is prominent followed by Green on both acquisition dates in the S2 control zone in contrast to control zone S1, where Green is the primary spectral region on both acquisition dates. Among vegetation indices, GNDVI demonstrated better separability capability than the other indices (NDVI and RENDVI) in the S2 control zone and on both acquisition dates whereas NDVI performed better results in the S1 control zone and both acquisition dates. Finally, the regression analysis revealed a second-order polynomial equation relating root weight to vegetation pixels (GNDVI) with R^2 = 0.34 whereas the average prediction is about 17.62% of the actual value (MAPE). The study shows that the multispectral data have limitations in discriminating between sugar beet cultivars and yield prediction. Further research should be conducted, considering the different phenological stages of the cultivars and multi-annual monitoring.

Keywords: sugar beet, cultivar discrimination, yield estimation, vegetation indices, UAVs multispectral imagery, Python programming language

INTRODUCTION

Crop monitoring and mapping are pivotal for addressing global challenges such as food security and climate change. Accurate and timely information on crop distribution is essential for making informed agricultural decisions, thereby ensuring global food security (Mahathi et al., 2023) With the global population rising and the adverse effects of climate change becoming more pronounced, effective crop monitoring and yield estimation are paramount. Remote Sensing plays a crucial role in monitoring crop health, growth stages, and overall agricultural productivity, which is critical for implementing strategies to mitigate the impacts of climate change on agriculture (Abuova et al., 2023). Remote sensing technology in agriculture presents an opportunity to address these challenges by providing extensive information on crop conditions throughout the entire season, thereby enabling well-informed management decisions (Darji et al., 2023). A vast amount of research exists in the literature regarding the use of remote sensing data in crop mapping and monitoring. Liu et al. (2020) conducted large-scale crop mapping in

the Qinghai region in China using multisource remote sensing satellite data from Landsat-8, Sentinel-2, and Sentinel-1 to map wheat, rapeseed, and corn crops with an ≈85% overall accuracy. Wu et al. (2017) combined very high spatial resolution aerial data (0.5 m) and hyperspectral data (EO1-Hyperion) to classify crops in Jiangsu province, China, achieving 95% overall accuracy. Gerhards et al. (2016) used thermal cameras and a VNIR/SWIR spectrometer to detect water stress in potato plants through various indices. They demonstrated that water stress detection in potato plants is feasible using indices calculated with remote sensing methods. Veysi et al. (2017) used Landsat-8 satellite data to calculate the crop water stress index (CWSI) for detecting plants under water stress and scheduling irrigation in sugarcane fields in Iran. They achieved R^2 values between 0.49 and 0.78 when comparing satellite data-derived CWSI with in-situ measurements. Furthermore, they measured the vegetation water content (VWC) and observed a negative relationship between the CWSI and VWC, which is directly related to the plants' age. Sakamoto (2020) introduced a new approach to crop yield estimation using a random forest regression (RF) algorithm integrated with environmental variables like temperature, precipitation, and soil moisture. This method, applied to corn and soybean yields in the U.S. with MODIS WDRVI (Wide Dynamic Range Vegetation Index) data, was compared to conventional linear (LM) and polynomial regression (PM) methods. The Random Forest (RF) approach outperformed LM and PM by better addressing biases and improving yield predictions in both irrigated and rainfed conditions, showcasing the potential of machine learning to enhance agricultural productivity forecasts. Tugrul (2021) used Landsat-8 's Operational Land Imager (OLI) data to calculate NDVI and combined it with soil properties to estimate sugar beet yield in Konya, Turkey. The study found a positive correlation between NDVI and sugar beet yield in late summer, with an R^2 value of 0.55

Given that crops are dynamic systems and their biophysical and biochemical factors change throughout the growing season, becomes apparent that time is an important variable in crop monitoring. Consequently, a factor of great importance is the period that the data will be captured. Nowadays, some problems in this direction (financial cost for airborne sensors, schedule for satellite imagery) can be resolved with the employment of UAVs (Zhang and Kovacs, 2012). Unmanned Aerial Vehicles (UAVs) are highly effective for crop monitoring due to the advanced embedded sensors they carry, such as multispectral, hyperspectral, thermal, and LIDAR sensors (Wang et al., 2022). UAVs are extensively used in the agriculture sector for various applications, including the detection of water stress in plants using thermal sensors (Sankaran et al., 2015). The insufficient irrigation system, and the uneven water distribution according to plants' needs, can cause water stress, where in this case leaf pores are closing, resulting in decreased photosynthesis and an increase in their temperature that leads to limited growth. Consequently, plants' temperature can be used as an indicator for water stress detection. Besides thermal infrared, spectral data (RGB, NIR), can be used for water stress detection in crops, given that it causes decreased growth and thus decreases biomass. It has been found a high correlation between the Normalized Difference Vegetation Index (NDVI) and yield production in control parcels with different irrigation levels (Walsh et al., 2023).

Detection of nutrient deficiencies, often resulting from poor fertilization or uneven distribution, is a crucial aspect of crop monitoring. Research on low nitrogen levels in maize using multispectral data from UAV-mounted sensors has shown a significant correlation between the Nitrogen Stress Index–NSI [*NSI (NDVI) = 1 – NDVIi/NDVIm*] and grain yield (Zaman-Allah et al., 2015). Agüera et al. (2011) found a high correlation (r = 0.8) between applied nitrogen (N) and NDVI in sunflowers using a UAV-mounted multispectral sensor. Despite various techniques used for detecting and monitoring crop diseases, the potential of UAV-obtained multispectral data remains underexplored. Jansen et al. (2014) correlated NDVI, Leaf Water Index (LWI), and Cercospora Leaf Spot Index (CLSI) with the severity of Cercospora in sugar beets. UAV imagery can also estimate growth factors like emergence vigor, Leaf Area Index (LAI), and biomass. Sankaran et al. (2014) found GNDVI highly correlated (r = 0.86) with

field measurements of wheat crop emergence. Hunt et al. (2010) found a linear correlation between GNDVI and LAI (R^2 = 0.85 for LAI values up to 2.5 m^2/m^2). UAV multispectral data are also used for crop yield estimation, with several studies correlating vegetation indices with yield production across various crops and growth stages. Khot et al. (2014) found correlations between yield production and GNDVI in wheat (r = 0.60-0.71). Stephen and Kumar (2023) used UAV multispectral images to distinguish weeds from sugar beet plants and evaluate sugar beet crop health in Rheinbach, Germany. They employed machine learning algorithms (Random Forest and Support Vector Machine) and object-based image analysis (OBIA) for crop and weed distinction, achieving 95-96% accuracy. They also used vegetation indices to create crop health maps. Jay et al. (2019) explored the benefits of centimetre-scale multispectral data for estimating biochemical and structural variables of sugar beet crops in France, concluding that green fraction (GF) and leaf chlorophyll content (Cab) provide better results than lower spatial resolution data (satellite imagery). Walsh et al. (2023) analyzed the impact of different water and nitrogen treatments and attempted yield and recoverable sugar estimation (ERS) on sugar beets in Germany, finding strong correlations between NDVI and root yield (R^2 = 0.91) and ERS (R^2 = 0.9).

The main objective of this paper was to investigate the utility of multispectral UAV imagery for discriminating between sugar beet cultivars and predicting yield. The Specific objectives were: i Evaluation of the separability of spectral bands and vegetation indices for 25 sugar beet cultivars using histogram correlation analysis, and ii. Investigating potential correlations between vegetation indices and yield.

MATERIALS AND METHODS

Region of interest – controlled field

The experimental field is located in Serres (Skotoussa village), Greece approximately 100 Km North East of Thessaloniki city (Figure 1). It was an experimental field owned by the Hellenic Sugar Industry (HSI), consisting of 25 different sugar beet cultivars. Each strip consisted of three sowing rows, spaced 50 cm apart. The total width of each strip was 2 meters, including a 0.5 m margin on each side. Each strip contained a single cultivar.

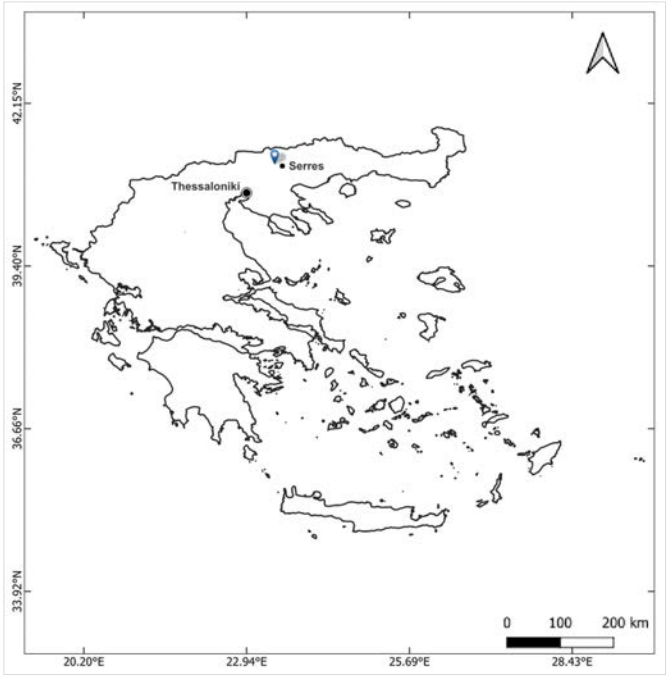

Figure 1. Region of interest

The experimental field was divided horizontally in the middle, so for every cultivar to be in different controlled zones, zone S2 (red) and zone S1 (yellow) (Figure 2).

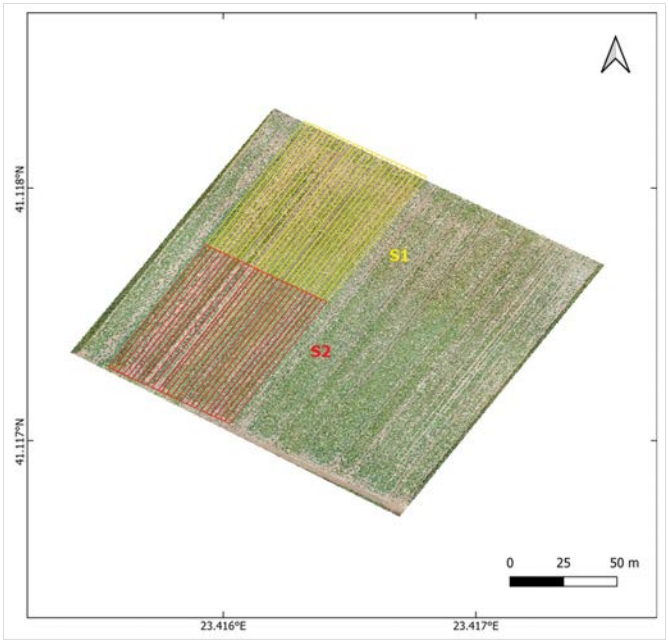

Figure 2. Experimental field and control zones

Two distinct operational protocols were implemented: S2, which includes comprehensive plant protection against Cercospora and nitrogen (N) fertilization, and S1, which entails minimal protection measures against Cercospora along with nitrogen (N) fertilization. Detailed specifications of these protocols, as followed by HSI, are classified and unavailable for disclosure by the authors. The study focuses exclusively on these two control zones (S1 and S2).

Fieldwork

UAVs' flights

The Multispectral data were obtained on two flight dates: August 25, 2017, and September 8, 2017, using a Parrot Sequoia multispectral sensor (Green: 550 nm, Red: 660 nm, Red Edge: 735 nm, NIR: 790 nm) mounted on an eBee fixed-wing UAV. The flight altitude was 120 m above ground level, resulting in a pixel size of ≈13 cm with 75% front and 65% side image acquisition overlap. Radiometric calibration target images were captured before the flight for white balance image calibration.

Field operations

Targets were placed in the field, to separate each strip of the different cultivars, their position was captured using a GPS receiver (Spectra Precision SP60) with RTK connected to the national HEPOS network (Delikaroglou, 2008). In addition, the precise delineation of the planting strips on the ground was performed using a GPS receiver. Furthermore, the Mobile Data Collection application (MDC) (GIS Cloud Ltd, Zagreb, Croatia), was used to capture the geotagged photos (Figure 3) of the 25 sugar beet cultivars on the experimental field.

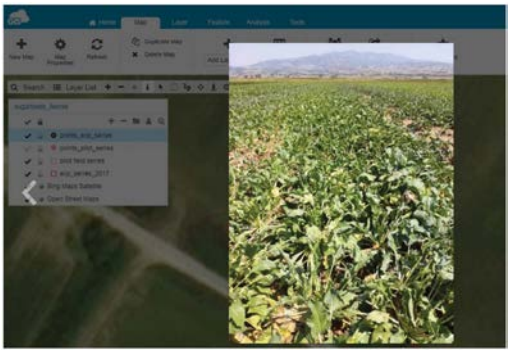

Figure 3. Geotagged image (field data collection)

Pre-processing

The raw multispectral image tiles were pre-processed with the use of Pix4DMapper software (Pix4D S.A., Prilly, Switzerland) and the utilization of the processing templates that are provided by the software. More specifically, the Ag Multispectral template was selected (Pix4D Documentation) along with white reference images. As a result, reflectance images were produced. After calculating the VIs using the QGIS software (QGIS project, 2000), a mask was applied on the reflectance images to remove the ground pixels using the threshold method

(Threshold value: $GNDVI_{August}$ = 0.4; $GNDVI_{September}$ = 0.38).

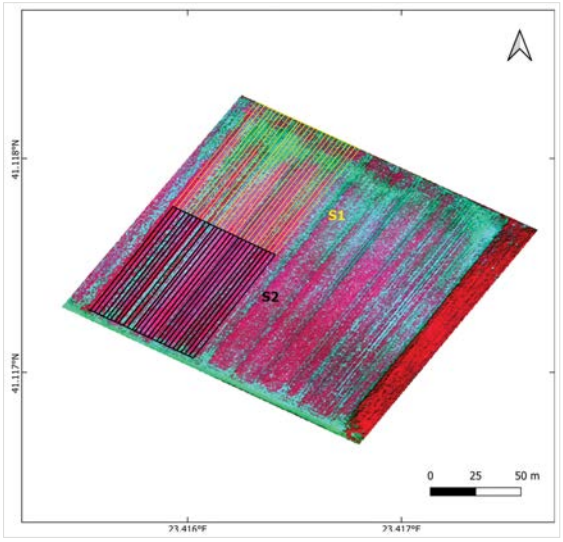

Figure 4. False Color composite image (RGB: NIR, R, G) - August

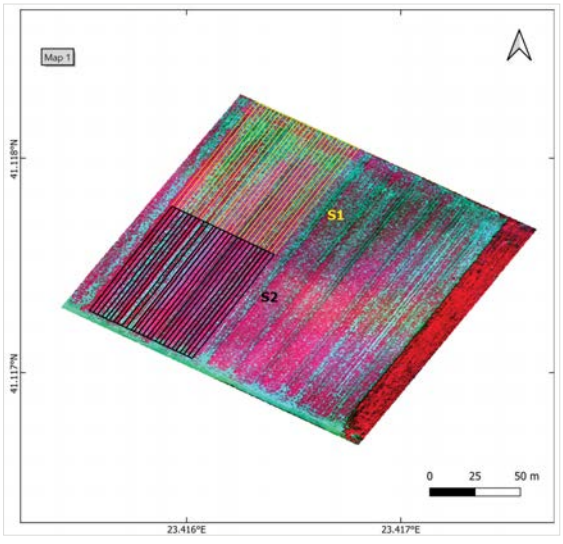

Figure 5. False Color composite image (RGB: NIR, R, G) - September

Data processing

Cultivars spectral discrimination using reflectance images

Spectral discrimination was implemented through the histogram comparison of respective spectral bands of the reflectance images in pairs for the 25 cultivars for both S1 and S2 controlled zones. For the histogram comparison, the open-source library OpenCV in a python environment (OpenCV development team, 2019). For the comparison, the histogram correlation algorithm (CV_COMP_CORREL) was used (Equation 1),

$$d(H_1, H_2) = \frac{\sum_I (H_1(I) - \bar{H_1})(H_2(I) - \bar{H_2})}{\sqrt{\sum_I (H_1(I) - \bar{H_1})^2 \sum_I (H_2(I) - \bar{H_2})^2}} \quad (1)$$

where:

$$\bar{H_k} = \frac{1}{N} \sum_J H_k(J)$$

and *N* is the total items that depict the range of the histogram.

Cultivars spectral discrimination using vegetation indices

The process followed for the cultivar's discrimination with the use of VIs, is the same one that was used for the discrimination with the use of reflectance images. The indices used for the discrimination of the cultivars are:

- NDVI (Normalized Difference Vegetation Index): NDVI = (NIR–RED)/(NIR+RED) (Rouse et al., 1973)
- GNDVI (Green Normalized Difference Vegetation Index): GNDVI = (NIR – GREEN) / (NIR + GREEN) (Gitelson et al., 1996)
- RENDVI (Red Edge Normalized Difference Vegetation Index):
  RENDVI = (NIR – Red Edge) / (NIR + Red Edge) (Sims and Gamon, 2002)

Crop yield estimation

The crop yield estimation was performed with the use of regression analysis between the number of "vegetation" pixels derived from VI's (GNDVI, NDVI, RENDVI) images of each cultivar (strips) and the actual roots weight derived from each strip (Diago et al., 2012). The method was applied in both control zones (S1 and S2) and acquisition dates (August and September).

RESULTS AND DISCUSSION

Cultivars discrimination based on reflectance data

August

After comparing histograms of the cultivars from data acquired in August, correlation matrices were produced for each spectral band, as shown in Figure 6 (an indicative correlation matrix for the NIR band). In this study, the thresholds for Pearson's correlation coefficient used for cultivar discrimination are defined as follows: r ≥ 0.7 indicates high correlation, 0.7 > r > 0.3 indicates moderate correlation, and r ≤ 0.3 indicates no correlation. Table 1 summarizes the range of Pearson's correlation coefficients for the discriminated cultivars across each spectral band.

Table 1. Range of Pearson's correlation coefficients for discriminated cultivars

Spectral band	S1		S2	
	min	max	min	max
	August			
Green	-0.18	0.29	0.04	0.29
Red	-0.28	0.3	-0.02	0.24
Red edge	-0.28	0.31	-0.29	0.3
NIR	-0.16	0.27	-0.18	0.3
	September			
Green	-0.26	0.29	-0.01	0.3
Red	0.29	0.29	-0.3	0.3
Red edge	0.11	0.3	-0.16	0.3
NIR	0.08	0.28	-0.12	0.3

The results showed that the majority of the cultivars are highly correlated with each other. Table 2 summarizes the cultivars that can be discriminated from all or some of the cultivars in each band. The Green band is the most effective for cultivar discrimination in control zone S1, as it discriminates four cultivars. In control zone S2, the NIR band is the most effective, even though it discriminates the same number of cultivars (four) as the Green and Red Edge bands.

NIR	Cultivar 1	Cultivar 2	Cultivar 3	Cultivar 4	Cultivar 5	Cultivar 6	Cultivar 7	Cultivar 8	Cultivar 9	Cultivar 10	Cultivar 11	Cultivar 12	Cultivar 13	Cultivar 14	Cultivar 15	Cultivar 16	Cultivar 17	Cultivar 18	Cultivar 19	Cultivar 20	Cultivar 21	Cultivar 22	Cultivar 23	Cultivar 24	Cultivar 25
Cultivar 1	1.00																								
Cultivar 2	**0.20**	1.00																							
Cultivar 3	0.67	0.69	1.00																						
Cultivar 4	0.73	0.56	0.77	1.00																					
Cultivar 5	**-0.03**	0.59	0.70	**0.22**	1.00																				
Cultivar 6	**0.21**	0.88	0.69	0.57	0.49	1.00																			
Cultivar 7	0.78	0.58	0.81	0.78	**0.24**	0.58	1.00																		
Cultivar 8	0.68	0.52	0.76	0.74	0.31	0.55	0.75	1.00																	
Cultivar 9	0.89	**0.13**	0.58	0.62	**-0.03**	**0.11**	0.70	0.57	1.00																
Cultivar 10	**-0.04**	0.78	0.49	0.33	0.63	0.75	0.35	0.37	**-0.09**	1.00															
Cultivar 11	0.92	**0.16**	0.63	0.71	**-0.01**	**0.16**	0.74	0.72	0.84	**-0.05**	1.00														
Cultivar 12	0.38	0.80	0.73	0.67	**0.30**	0.89	0.68	0.65	**0.24**	0.63	0.33	1.00													
Cultivar 13	**-0.12**	0.86	0.47	0.31	0.61	0.82	0.32	**0.27**	**-0.17**	0.46	**-0.18**	0.69	1.00												
Cultivar 14	**0.17**	0.87	0.66	0.54	0.41	0.93	0.54	0.50	**0.09**	0.74	**0.10**	0.91	0.84	1.00											
Cultivar 15	**0.18**	0.89	0.68	0.57	0.46	0.93	0.54	0.53	**0.08**	0.75	**0.12**	0.89	0.85	0.95	1.00										
Cultivar 16	0.41	0.87	0.79	0.69	0.45	0.90	0.72	0.67	**0.29**	0.69	0.37	0.92	0.74	0.90	0.90	1.00									
Cultivar 17	0.89	**0.21**	0.65	0.69	**0.02**	**0.22**	0.74	0.69	0.80	**-0.01**	0.87	0.37	**-0.09**	**0.17**	**0.18**	0.40	1.00								
Cultivar 18	**-0.05**	0.87	0.54	0.38	0.54	0.88	0.38	**0.30**	**-0.10**	0.78	**-0.12**	0.76	0.93	0.91	0.90	0.80	**-0.04**	1.00							
Cultivar 19	0.63	0.75	0.83	0.80	0.31	0.80	0.82	0.81	0.49	0.54	0.60	0.90	0.53	0.79	0.80	0.90	0.59	0.61	1.00						
Cultivar 20	0.75	0.65	0.83	0.84	**0.24**	0.67	0.83	0.79	0.65	0.40	0.70	0.78	0.40	0.66	0.66	0.80	0.71	0.48	0.89	1.00					
Cultivar 21	**0.21**	0.90	0.69	0.58	0.47	0.92	0.57	0.51	**0.10**	0.77	**0.14**	0.89	0.85	0.94	0.93	0.90	**0.20**	0.90	0.78	0.69	1.00				
Cultivar 22	0.31	0.85	0.74	0.65	0.46	0.91	0.65	0.68	**0.19**	0.73	**0.30**	0.93	0.75	0.90	0.90	0.93	0.33	0.81	0.88	0.76	0.90	1.00			
Cultivar 23	**0.26**	0.81	0.67	0.59	0.50	0.85	0.60	0.66	**0.13**	0.72	**0.27**	0.87	0.72	0.83	0.85	0.87	**0.30**	0.75	0.82	0.69	0.84	0.91	1.00		
Cultivar 24	**-0.12**	0.85	0.48	0.31	0.61	0.85	0.32	**0.30**	**-0.16**	0.80	**-0.18**	0.70	0.92	0.85	0.86	0.74	**-0.10**	0.94	0.54	0.40	0.86	0.77	0.72	1.00	
Cultivar 25	0.70	0.69	0.84	0.84	**0.24**	0.74	0.82	0.79	0.58	0.46	0.67	0.86	0.44	0.74	0.73	0.85	0.66	0.54	0.93	0.90	0.74	0.82	0.75	0.46	1.00

Figure 6. Correlation matrix (Image acquisition: August, S2 control zone, NIR Band)

Table 2. Discriminated cultivars in every band, first flight date (25 August 2017)

Spectral band	Discriminated cultivars S1		Discriminated cultivars S2	
	Cultivar	Discriminated from cultivars	Cultivar	Discriminated from cultivars
Green	4	All	6	11,12,20
	5	4,6,12,14,15,16,18,19,20,24	12	6,8,21
	7	4,12,14,15,16,18,19,20,24,25	20	6,8,21
	9	4,12,14,15,16,18,19,20,24	21	11,12,20
Red	13	All except 20th	15	1,6,7,8,9,17
			18	1,6,7,8,9,17
Red Edge	21	All except 1st and 3rd	1	5,10,11,13,18,19,21,23
			4	10,13,21,24
			9	2,5,10,12,13,14,18,19,22,23
			11	10,13,18,19,21,23
NIR	21	All except 1st and 3rd	1	2,5,10,13,14,15,18,21,23,24
			9	2,5,10,12,13,14,15,16,18,21,22,23,24
			11	2,5,10,13,14,15,18,21,23,24
			17	2,5,10,13,14,15,18,21,24

This is due to the NIR band's ability to distinguish these four cultivars from a larger number of other cultivars. Cultivar 21 can be discriminated from most of the other cultivars using the Green, Red Edge, and NIR bands in both control zones. Cultivars 13, 14, and 15 can be discriminated from other cultivars using the Red Edge and NIR bands in S2. Additionally, cultivar 14 can be discriminated from some other cultivars in S1 using the Green band. Cultivar 13 can also be discriminated from the rest of the cultivars in S1 using the Red band. Cultivar four (4) can be discriminated from the rest using the Green band in S1. Finally, cultivar five (5) can be discriminated from some others using the

Green band in S1 and the Red Edge and NIR bands in S2. A pattern emerges showing that certain cultivars in both S1 and S2 control zones are discriminated from common cultivars (discrimination overlap) using certain bands, as summarized in Table 4.

September

In the image captured in September, there is a notable increase in the number of cultivars that are highly correlated. As a result, discrimination between them becomes more challenging at the later growth stage. The cultivars that can still be discriminated against are listed in Table 3. The results indicate that a greater number of cultivars can be discriminated in the second control zone (S2), where full plant protection was implemented, compared to the first control zone (S1), where only partial plant protection was applied.

In the S1 control zone, the Green band is particularly effective, allowing for the discrimination of three cultivars from others. In the S2 control zone, the Green band remains the most effective, enabling the discrimination of five cultivars. This is followed by the Red and Red Edge bands, which also contribute to cultivar discrimination but are less prominent compared to the Green band. Also, cultivar five (5) appears to be discriminated against by others using the Red edge and NIR bands, while cultivar 13 can be discriminated against by others using the Green and Red bands. Lastly, some overlap in cultivar discrimination is observed in the September dataset, affecting both the S1 and S2 control zones (Table 4).

Table 3. Discriminated cultivars in every band, second flight date (08 September 2017)

Spectral band	Discriminated cultivars S1		Discriminated cultivars S2	
	Cultivar	Discriminated from cultivars	Cultivar	Discriminated from cultivars
Green	9	3,4,7,8,11,12,14,21,23,25	*6*	*2,11,12,13,14*
	20	2,3,6,7,8,12,14,15,16,17,18,21,23,25	8	2,11,12,13,14
			10	2,12,13,14
	24	2,3,6,7,8,12,15,16,17,18,21,23,25	13	3,4,5,6,8,9,10,17,19,21,22,23,24
			14	4,5,6,8,10,17,19,21,22,23,24
Red	7	10	12	7,8,17,22,23,25
			13	6,7,8,17,22,23,24,25
			18	7,8,17,22,23,24
			24	2,4,13,14,15,18,20,21
Red Edge	1	5,24	5	7,16,17,22,23
			7	4,5,9,14,25
	24	25	17	3,4,5,6,9,14,15,20,21,24,25
			23	3,4,5,6,9,14,25
NIR	24	11,15	5	7,9,11,12,22,24
			11	2,3,4,5,13,14,18,20,25
	25	5,11	12	2,3,4,5,13,14,18,20,25

Table 4. Reflectance data, common cultivar discrimination (discrimination overlap)

Spectral band	S1		S2	
	Discriminated cultivars	Overlap (%)	Discriminated cultivars	Overlap (%)
			August	
Green	5, 7, 9	36%	6, 21	12%
			12, 20	12%
Red	-	-	15, 18	24%
Red edge	-	-	1, 9, 11	28%
NIR	-	-	1, 9, 11, 17	36%
			September	
Green	9, 20, 24	32%	6, 8, 10	12%
			13, 14	44%
Red			12, 13, 18	24%
Red edge			7, 17, 23	20%
NIR			11, 12	36%

Cultivars discrimination based on vegetation indices

NDVI histogram comparison

The NDVI comparison results from August reveal that most cultivars are highly correlated with one another. The Pearson's correlation coefficient range for the discriminated cultivars for each Vegetation Index is summarized in the following table (Table 5).

Table 5. Range of Pearson's correlation coefficients for discriminated cultivars based on vegetation indices

Vegetation indices	S1		S2	
	min	max	min	max
		August		
NDVI	-0.28	0.29	-0.27	0.3
RENDVI	0.21	0.28	-0.05	0.3
GNDVI	-0.18	0.29	-0.3	0.3
		September		
NDVI	-0.27	0.3	-0.3	0.29
RENDVI	0.1	0.22	-0.23	0.29
GNDVI	-0.19	0.3	-0.26	0.3

Despite the high correlations that existed among the cultivars, as shown in Table 6, Cultivar 10 stands out as it can be discriminated from the majority of the other cultivars across both acquisition dates and control zones. Similarly, Cultivars one (1) and four (4) can be discriminated from some other cultivars in both control zones and dates. In contrast, Cultivar six (6) can be discriminated from others during the mid-season growth stage in August but not in the late growth stages of September.

GNDVI histogram comparison

The GNDVI comparison revealed predominantly high and medium correlations among the cultivars across both acquisition dates and control zones. The cultivars that can be discriminated against are summarized in Table 7. Cultivars one (1) and 10 can be discriminated against by others in both control zones and dates. Cultivar four (4) can be discriminated from the majority of other cultivars in the S2 control zone across both acquisition dates. Additionally, in the S1 control zone, Cultivar Four (4) is discriminated from Cultivars One (1), Seven (7), and Nine (9) in August, and from Cultivar One (1) in September.

Table 6. NDVI comparison discriminated cultivars

Vegetation index	Discriminated cultivars S1		Discriminated cultivars S2	
	Cultivar	Discriminated from cultivars	Cultivar	Discriminated from cultivars
NDVI (August)	1	5,6,12,21,22	1	5,6
	4	2,7,8,9,13,14,15,16,17,18,23,24,25	4	3,6,8,12,13,20,21,22
	6	1,2,7,9,15,17,18,19,20,24	6	4,7,8,24
	10	2,8,9,11,12,13,14,15,16,17,23,25	10	2,8,9,11,13,14,15,16,17,18,19,20,22,23,25
	19	6,21,22	24	5,6,12,13,20
NDVI (September)	1	3,5,6,11,12,13,14,16,21,22,23,25	1	6,12,13
	4	2,7,15,17,18,19,20,24	4	3,6,8,11,12,13,16,17,20,21,22,23,25
	10	All except 6th and 22nd		
	24	4,5,10	10	All except 5th and 12th

Table 7. GNDVI comparison discriminated cultivars

Vegetation index	Discriminated cultivars S1		Discriminated cultivars S2	
	Cultivar	Discriminated from cultivars	Cultivar	Discriminated from cultivars
GNDVI (August)	1	4,5,6,11,12,13	1	5,10,12,13,20
			4	2,3,6,11,14,15,16,17,18,19,21,22,23,25
	7	4,6,10,12,13	7	5,6,10,12,13,20,21
			8	2,5,6,10,12,16,17,18,19,21,22,25
	9	4,6,10,12,13	10	1,7,8,9,11,14,15,23,24
	10	2,7,8,9,18,19,20,21,24	12	1,7,8,9,24
			13	1,7,9,14,15,23,24
GNDVI (September)	1	4,5,6,11,12,14,15,16,17,22,25	4	2,3,6,8,9,11,14,15,16,17,18,19,20,21,22,25
			8	4,5,6,10,12,13,16,20
	10	2,3,7,8,9,18,19,20,21,24	10	1,2,3,7,8,9,14,15,18,19,21,22,24,25
	13	2,3,7,8,9,18,19,20,21,24	13	1,2,7,8,9,15,17,18,24

Finally, Cultivar 13 can be discriminated from some other cultivars in both zones and dates, with the best results observed during the late growth stages.

RENDVI histogram comparison

The RENDVI histogram comparison revealed high correlations among the cultivars, making it the least effective for cultivar discrimination compared to NDVI and GNDVI across both acquisition dates and control zones. The results, presented in Table 8, indicate that Cultivar 18 is the only cultivar that can be discriminated in both dates within the S2 control zone.

Table 8. RENDVI comparison discriminated cultivars

Vegetation index	Discriminated cultivars S1		Discriminated cultivars S2	
	Cultivar	Discriminated from cultivars	Cultivar	Discriminated from cultivars
RENDVI (August)	9	2,3,5,6,13	18	11,14,15,16,24
			20	9,11,14,15,16,23,24,25
RENDVI (September)	8	21,22,23,24	17	9,24,25
			18	2,3,9,11,24,25
			19	2,3,9,11,25

The following Table 9 summarizes the cultivars that showed discrimination overlap, through VIs histogram comparison, for both acquisition dates and control zones.

In summary, the histogram comparison of the cultivars' reflectance data reveals that spectral bands can effectively discriminate some cultivars, depending on the acquisition dates and treatment conditions. NDVI and GNDVI have proven to be particularly useful for cultivar discrimination across various conditions. Notably, the S2 control zone consistently shows superior results, with clearer cultivar separation. This improvement is likely due to differences in treatments, irrigation practices, plant density, or other factors between the S1 and S2 zones (Hoffmann and Blomberg, 2004). Further investigation is needed to pinpoint the specific factors influencing these results.

The findings of this research regarding cultivar discrimination are consistent with those of Galidaki et al. (2021), who utilized UAVs and vegetation indices (VIs) to discriminate and map vine varieties in Greece. They concluded that multispectral data do not effectively discriminate cultivars of the same species.

Table 9. VIs common cultivar discrimination (discrimination overlap)

Vegetation Index	S1		S2	
	Discriminated cultivars	Overlap (%)	Discriminated cultivars	Overlap (%)
			August	
NDVI	4, 10	40%	4, 10	16%
			1, 7	20%
GNDVI	1, 7, 9	20%	4, 8	36%
			10, 13	28%
RENDVI	-	-	18, 20	20%
			September	
NDVI	1, 10	48%	1, 4, 10	12%
GNDVI	10, 13	40%	4, 10	44%
			4,10, 13	24%
RENDVI	-	-	17, 18	12%
			18, 19	20%

In contrast, hyperspectral data have demonstrated a higher capacity for discrimination. For instance, Galvão et al. (2006) showed that hyperspectral data (Hyperion/EO-1) achieved a discrimination accuracy of 87% for sugarcane varieties in Brazil, whereas the best results with multispectral data, such as those from the Enhanced Thematic Mapper Plus (ETM+) on Landsat-7 and the Moderate Resolution Imaging Spectroradiometer (MODIS/Terra), reached only 74% accuracy. This indicates that hyperspectral data provide superior discrimination of cultivars compared to multispectral approaches.

Crop yield estimation

Crop yield estimation based on vegetation indices

According to regression analysis, performed between vegetation indices and actual yield metrics (root weight), GNDVI showed better results in comparison with NDVI and RENDVI, in the S2 control zone (August). Must be noted that the cultivars four (4), five (5), eight (8) and 15, were not used for the estimation (outliers). The regression analysis yielded the following second-order polynomial equation relating root weight to vegetation pixels.

$$y = -0.0003x^2 + 2.929x + 1209.5 \quad (2)$$

$$R^2 = 0.3384$$

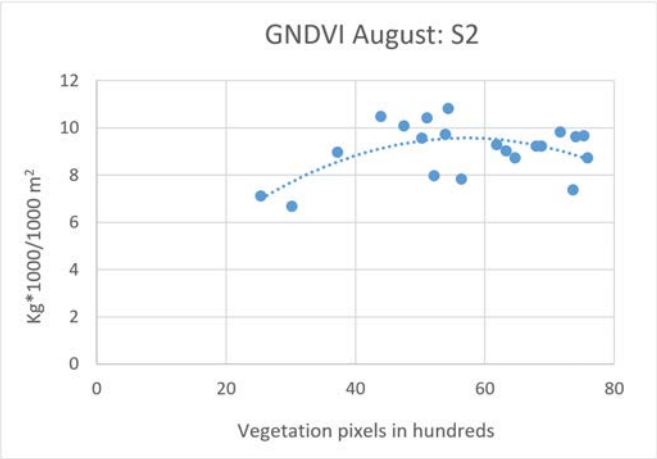

Figure 7. Regression analysis plot

While there is a relationship between vegetation pixels and root weight, a significant portion of the variability in root weight remains unexplained by the model. Despite the model explaining only a portion of the variability in root weight, it still provides good predictions, with the average prediction being within about 17.62% of the actual value.

The MAPE was used in the present study, as it is commonly used when the quantity to predict, is known to be above zero (De Myttenaere et al., 2016). In addition, MAPE constitutes a well-fitted method, in order to check the prediction results (Khair et al., 2017). For the validity check of the equation, the Mean Absolute Percentage Error (MAPE) was calculated as shown in the following equation (Equation 3).

$$\text{MAPE} = \frac{100}{n}\sum_{i=1}^{n}\left|\frac{yi-\widehat{yi}}{yi}\right| \quad (3)$$

where y_i is the actual value, $\hat{y}_i$ is the estimated value and n is the total number of samples used.

The estimated root weight, derived from the regression analysis, resulted to MAPE = 17.62% (MAPE <10%: Highly accurate forecasting, 10–20%: Good forecasting, 20–50%: Reasonable forecasting, >50%: Inaccurate forecasting). According to (Ostertagová, 2012) the MAPE is the most useful index for estimation validity check, as it is used for the relative performance.

The results of this study align with the findings of Kyratzis et al. (2017) in Cyprus, who demonstrated that GNDVI is effective for yield prediction in wheat. Similarly, the results are consistent with those of Kayad et al. (2019), who identified a correlation between GNDVI and yield variability in corn.

Moreover, the literature indicates that for accurate crop yield prediction, spectral data should be collected before the plants reach their final growth stage. Early crop stages are preferred because, at later stages, factors such as canopy development, weed infestation, and plant diseases can vary significantly and impact the accuracy of predictions (Hoffmann and Blomberg, 2004).

CONCLUSIONS

This research evaluated the effectiveness of multispectral UAV imagery for discriminating between 25 sugar beet cultivars and predicting yield. The findings revealed that multispectral data have limitations in both discriminating cultivars and predicting yield. Specifically, the NIR band emerged as the most significant spectral region for these tasks, followed by the Green band, particularly in the S2 control zone. In contrast, the Green band was more dominant in the S1 control zone across both acquisition dates.

Among the vegetation indices assessed, GNDVI demonstrated superior discriminative power compared to NDVI and RENDVI in the S2 control zone and across both acquisition dates. Conversely, NDVI performed better in the S1 control zone during both acquisition periods. Additionally, regression analysis identified a second-order polynomial relationship between root weight and vegetation pixels (GNDVI), with an R^2 value of 0.34. While this model accounts for only a portion of the variability in root weight, it provides reliable predictions with an average accuracy of approximately 17.62% relative to the actual values.

Further research is needed to explore different phenological stages of the cultivars and to conduct multi-annual monitoring to enhance the accuracy and applicability of these predictive models.

ACKNOWLEDGEMENTS

The authors would like to express their gratitude to GeoSense private company, Greece and specifically to Vasilios Polychronos, CTO of GeoSense for their support in UAV image acquisition. We would also like to thank the Hellenic Sugar Industry (HSI) and more specifically Dr. Georgios Kokinis, Director of the Agricultural Department of HSI for providing ground truth data and experimental design.

REFERENCES

Abuova, A., Tulkubayeva, S., Tulayev, Y., Somova, S., Sidorik, A., Hunger, O., Zinchenko, A., Vykhodtsev, V. (2023) The use of remote sensing, ground survey and the yield mapping system in the conditions of northern Kazakhstan for food production and food security. Food Science and Technology, 43, e76321. DOI: https://doi.org/10.1590/fst.76321

Agüera, F., Carvajal, F., Pérez, M. (2011) Measuring sun-flower nitrogen status from an unmanned aerial vehicle-based system and an on the ground device. The International Archives of the Photogrammetry, Remote Sensing and Spatial Information Sciences, 38, 33–37. DOI: https://doi.org/10.5194/isprsarchives-XXXVIII-1-C22-33-2011

Darji, P., Desai, N., Bhavsar, D., & Pandya, H. (2023) A review: Applications of remote sensing in agriculture. International Association of Biologicals and Computational Digest, 2 (1), 108–117. DOI: https://doi.org/10.56588/iabcd.v2i1.137

Delikaroglou, D. (2008) The Hellenic Positioning System (HEPOS) and its foreseeable implications on the spatial data infrastructure in Greece. Technical Chronicles Scientific, J, 1-2.

De Myttenaere, A., Golden, B., Le Grand, B., Rossi, F. (2016) Mean absolute percentage error for regression models. Neurocomputing, 192, 38-48. DOI: https://doi.org/10.1016/j.neucom.2015.12.114

Diago, M. P., Correa, C., Millán, B., Barreiro, P., Valero, C., Tardaguila, J. (2012) Grapevine yield and leaf area estimation using supervised classification methodology on RGB images taken under field conditions. Sensors, 12 (12), 16988-17006. DOI: https://doi.org/10.3390/s121216988

Galidaki, G., Panagiotopoulou, L., Vardoulaki, T. (2021) Use of UAV-borne multispectral data and vegetation indices for discriminating and mapping three indigenous vine varieties of the Greek Vineyard. Journal of Central European Agriculture, 22 (4), 762-770. DOI: https://doi.org/10.5513/JCEA01/22.4.2754

Galvão, L. S., Formaggio, A. R., Tisot, D. A. (2006) The influence of spectral resolution on discriminating Brazilian sugarcane varieties. International Journal of Remote Sensing, 27 (4), 769-777. DOI: https://doi.org/10.1080/01431160500166011

Gerhards, M., Rock, G., Schlerf, M., Udelhoven, T. (2016) Water stress detection in potato plants using leaf temperature, emissivity, and reflectance. *International journal of applied Earth observation and geoinformation*, 53, 27-39. DOI: https://doi.org/10.1016/j.jag.2016.08.004

Gitelson, A. A., Kaufman, Y. J., Merzlyak, M. N. (1996) Use of a green channel in remote sensing of global vegetation from EOS-MODIS. Remote sensing of Environment, 58 (3), 289-298. DOI: https://doi.org/10.1016/S0034-4257(96)00072-7

Hoffmann, C. M., Blomberg, M. (2004) Estimation of leaf area index of Beta vulgaris L. based on optical remote sensing data. Journal of agronomy and crop science, 190 (3), 197-204. DOI: https://doi.org/10.1111/j.1439-037X.2004.00093.x

Hunt, E.R., Hively, W.D., Fujikawa, S.J., Linden, D.S., Daughtry, C.S., McCarty, G.W. (2010) Acquisition of NIR-green-blue digital photographs from unmanned aircraft for crop monitoring. Remote Sensing, 2 (1), 290–305. DOI: https://doi.org/10.3390/rs2010290

Jansen, M., Bergsträsser, S., Schmittgen, S., Müller-Linow, M., Rascher, U. (2014) Noninvasive spectral phenotyping methods can improve and accelerate cercospora disease scoring in sugar beet breeding. Agriculture, 4 (2), 147–158. DOI: https://doi.org/10.3390/agriculture4020147

Jay, S., Baret, F., Dutartre, D., Malatesta, G., Héno, S., Comar, A., Weiss, M. Maupas, F. (2019) Exploiting the centimeter resolution of UAV multispectral imagery to improve remote-sensing estimates of canopy structure and biochemistry in sugar beet crops. Remote Sensing of Environment, 231, 110898. DOI: https://doi.org/10.1016/j.rse.2018.09.011

Kayad, A., Sozzi, M., Gatto, S., Marinello, F., Pirotti, F. (2019) Monitoring within-field variability of corn yield using Sentinel-2 and machine learning techniques. Remote Sensing, 11 (23), 2873. DOI: https://doi.org/10.3390/rs11232873

Khair, U., Fahmi, H., Al Hakim, S., Rahim, R. (2017, December) Forecasting error calculation with mean absolute deviation and mean absolute percentage error. *In journal of physics: conference series* (Vol. 930, No. 1, p. 012002) IOP Publishing. DOI: https://doi.org/10.1088/1742-6596/930/1/012002

Khot, L. R., Sankaran, S., Cummings, T., Johnson, D., Carter, A. H., Serra, S., Musacchi, S. (2014) Applications of unmanned aerial system in Washington state agriculture, Paper No. 1637. In: Proceedings of the 12th International Conference on Precision Agriculture, Sacramento, CA, USA, 20–23 July 2014, International Society of Precision Agriculture, pp. 20-23.

Kyratzis, A. C., Skarlatos, D. P., Menexes, G. C., Vamvakousis, V. F., Katsiotis, A. (2017) Assessment of vegetation indices derived by UAV imagery for durum wheat phenotyping under a water limited and heat stressed Mediterranean environment. Frontiers in Plant Science, 8, 1114. DOI: https://doi.org/10.3389/fpls.2017.01114

Liu, X., Zhai, H., Shen, Y., Lou, B., Jiang, C., Li, T., Hussain, S.B., Shen, G. (2020) Large-scale crop mapping from multisource remote sensing images in google earth engine. IEEE Journal of Selected Topics in Applied Earth Observations and Remote Sensing, 13, 414-427. DOI: https://doi.org/10.1109/JSTARS.2019.2963539

Mahathi, G., Sumanjali, B. C., Abhinaya, P., Venkatesan, M. (2023) Crop Mapping using Multispectral Sentinel-2 Dataset. International Reasearch Journal on Advanced Science Hub, 5 (05), 507–512 DOI: https://doi.org/10.47392/irjash.2023.S068

OpenCV development team. (2019) OpenCV documentation (Release 2.4.13.7) OpenCV development team.

Ostertagová, E. (2012) Modelling using polynomial regression. Procedia Engineering, 48, 500-506. DOI: https://doi.org/10.1016/j.proeng.2012.09.545

Pix4D S.A. (n.d.) How to process Sequoia imagery - PIX4Dmapper. Pix4D Documentation. Available at: https://support.pix4d.com/hc/en-us/articles/209362146-How-to-process-Sequoia-imagery-PIX4Dmapper#label3 [Accessed 15 April 2024].

QGIS project (2020) Quantum GIS (Release 3.16.11 Hannover) QGIS project.

Rouse, Jr. J. W., Haas, R. H., Schell, J. A., Deering, D. W. (1973) Monitoring the vernal advancement and retrogradation (green wave effect) of natural vegetation (No. NASA-CR-132982).

Sakamoto, T. (2020) Incorporating environmental variables into a MODIS-based crop yield estimation method for United States corn and soybeans through the use of a random forest regression algorithm. ISPRS Journal of Photogrammetry and Remote Sensing, 160, 208-228. DOI: https://doi.org/10.1016/j.isprsjprs.2019.12.012

Sankaran, S., Khot, L.R., Carter, A.H., Garland-Campbell, K. (2014) Unmanned aerial systems based imaging for field-based crop phenotyping: winter wheat emergence evaluation, Paper No. 1914284. In: 2014 ASABE Annual International Meeting, Montreal, Quebec, Canada, July 13–14.

Sankaran, S., Khot, L. R., Espinoza, C. Z., Jarolmasjed, S., Sathuvalli, V. R., Vandemark, G. J., Miklas, P.N., Carter, A.H., Pumphrey, V.R., Knowls, N.R. Pavek, M. J. (2015) Low-altitude, high-resolution aerial imaging systems for row and field crop phenotyping: A review. European Journal of Agronomy, 70, 112-123. DOI: https://doi.org/10.1016/j.eja.2015.07.004

Sims, D. A., Gamon, J. A. (2002) Relationships between leaf pigment content and spectral reflectance across a wide range of species, leaf structures and developmental stages. Remote sensing of environment, 81 (2-3), 337-354. DOI: https://doi.org/10.1016/S0034-4257(02)00010-X

Stephen, S., Kumar, V. (2023) Detection and analysis of weed impact on sugar beet crop using drone imagery. Journal of the Indian Society of Remote Sensing, 51 (12), 2577-2597. DOI: https://doi.org/10.1007/s12524-023-01782-1

Tugrul, K. (2021) Estimation of sugar beet biomass and yield comparing NDVI measurements and physical soil parameters. Sugar Ind.-Zuckerind, 146, 100-109. DOI: https://doi.org/10.36961/si26238

Veysi, S., Naseri, A. A., Hamzeh, S., Bartholomeus, H. (2017) A satellite based crop water stress index for irrigation scheduling in sugarcane fields. Agricultural water management, 189, 70-86. DOI: https://doi.org/10.1016/j.agwat.2017.04.016

Walsh, O. S., Nambi, E., Shafian, S., Jayawardena, D. M., Ansah, E. O., Lamichhane, R., McClintick-Chess, J. R. (2023) UAV-based NDVI estimation of sugarbeet yield and quality under varied nitrogen and water rates. Agrosystems, Geosciences & Environment, 6 (1), e20337. DOI: https://doi.org/10.1002/agg2.20337

Wang, Q., Che, Y., Shao, K., Zhu, J., Wang, R., Sui, Y., Guo, Y., Li, B., Meng, L. Ma, Y. (2022) Estimation of sugar content in sugar beet root based on UAV multi-sensor data. Computers and Electronics in Agriculture, 203, 107433. DOI: https://doi.org/10.1016/j.compag.2022.107433

Wu, M., Huang, W., Niu, Z., Wang, Y., Wang, C., Li, W., Hao, P., Yu, B. (2017) Fine crop mapping by combining high spectral and high spatial resolution remote sensing data in complex heterogeneous areas. Computers and Electronics in Agriculture, 139, 1-9. DOI: https://doi.org/10.1016/j.compag.2017.05.003

Zaman-Allah, M., Vergara, O., Araus, J. L., Tarekegne, A., Magorokosho, C., Zarco-Tejada, P. J., Hornero, A., Albà, A.H., Das, B., Craufurd, P., Olsen, M., Prasanna, B.M., Cairns, J. (2015) Unmanned aerial platform-based multi-spectral imaging for field phenotyping of maize. Plant Methods, 11, 1-10. DOI: https://doi.org/10.1186/s13007-015-0078-2

Zhang, C., Kovacs, J.M. (2012) The application of small unmanned aerial systems for precision agriculture: a review. Precision Agriculture, 13, 693–712. DOI: https://doi.org/10.1007/s11119-012-9274-5